Dalton Transactions

PAPER

View Article Online
View Journal | View Issue

Cite this: *Dalton Trans.*, 2015, **44**, 15014

Field-induced slow relaxation of magnetization in a pentacoordinate Co(II) compound [Co(phen)(DMSO)Cl_2]†

Ivan Nemec,[a] Raphael Marx,[b] Radovan Herchel,[a] Petr Neugebauer,[b] Joris van Slageren[b] and Zdeněk Trávníček*[a]

Received 8th June 2015,
Accepted 16th July 2015

DOI: 10.1039/c5dt02162f

www.rsc.org/dalton

The static and dynamic magnetic properties of a pentacoordinate [Co(phen)(DMSO)Cl_2] compound (phen = 1,10′-phenanthroline, DMSO = dimethyl sulfoxide) were thoroughly studied by experimental (SQUID magnetometry and HF-EPR spectroscopy) and theoretical methods (DFT and CASSCF calculations). It has been found from temperature/field-dependent magnetization measurements that the studied compound possesses a large and negative magnetic anisotropy (D = –17(1) cm^{-1}) with large rhombicity (E/D = 0.24(5)), and these experimental results are in agreement with *ab initio* calculations (D = –17.7 cm^{-1}, E/D = 0.31). Interdoublet resonances were not observed in the HF-EPR measurements, but the large rhombicity was confirmed (D_{EPR} = –17.7 cm^{-1} (fixed from CASSCF calculations), E/D_{EPR} = 0.33). A frequency dependent out-of-phase susceptibility signal was observed only in a non-zero static magnetic field (B = 0.1 T) and the following parameters of slow-relaxation of magnetisation were derived from the experimental data: either the energy of spin reversal barrier, U_{eff} = 10.4 K, and the relaxation time, $\tau_0 = 5.69 \times 10^{-9}$ s using the Debye model, or U_{eff} = 21.4–40.3 K and $\tau_0 = 0.248–58.3 \times 10^{-9}$ based on a simplified model.

Introduction

Single-molecule magnets (SMMs) are molecular compounds in which each molecule exhibits slow-relaxation of magnetisation and thus it behaves as a molecular nanomagnet. The energy barrier of spin reversal is defined as $\Delta = |D|(S^2 - 1/4)$ for odd values of the ground spin state S, under the condition that D is negative. This means that magnetic anisotropy is uniaxial and, in the case of Co(II) with S = 3/2, the lowest energy level of the ground state is the Kramers doublet |±3/2> and the energy separation from the adjacent Kramers doublet |±1/2> is equal to $2D$.[1]

SMMs were discovered 24 years ago with the famous Mn12 compound[2] and it was believed for a long time that the total spin might be an important variable regarding spin reversal barrier (U_{eff}) which defines the basic properties of SMMs. However, it has turned out that magnetic anisotropy is the key factor in the design of SMM compounds and this was further confirmed by the discovery of the first mononuclear lanthanide SMM[3] and other theoretical studies.[4] Other coordination compounds containing only one paramagnetic metal centre and exhibiting slow-relaxation of magnetization followed: Fe(I[5]/II[6]/III[7]), Ni(I)[8] or Mn(III).[9]

The first two mononuclear Co(II) compounds exhibiting slow-relaxation of magnetization were reported by Jurca *et al.* in 2011.[10] Both compounds were pentacoordinate possessing a distorted square-pyramidal geometry with bis(imino)pyridine and thiocyanido ligands ([Co(bip1)$(NCS)_2$] (**I**), [Co(bip2)$(NCS)_2$] (**II**), where bip1 = [2,6-bis{1-[(2,6-diisopropylphenyl)imino]-ethyl}pyridine], bip2 = [2,6-bis{1-[(2,6-diisopropylphenyl)-imino]benzyl}pyridine]). This discovery was followed by further reports on SMM behaviour in tetra-,[11] penta-,[12] hexa-[13] or heptacoordinate[14] Co(II) compounds, but in most of the cases, the slow relaxation of magnetisation was observed only in a non-zero static magnetic field. Only a few examples of slow-relaxation of the magnetisation in pentacoordinate Co(II) compounds have been reported,[15] in all cases described as compounds consisting of a tridendate heterocyclic *N*-donor ligand and two halido or pseudohalido ligands: [Co(bpp)Cl_2] (**III**),[16] [Co(terpy)Cl_2] (**IV**) and [Co(terpy)$(NCS)_2$] (**V**)[17] (terpy = terpyridine, bpp = 4-hept-1-ynyl-2,6-dipyrazol-1-ylpyridine). Remark-

[a]*Regional Centre of Advanced Technologies and Materials, Department of Inorganic Chemistry, Faculty of Science, Palacký University, 17. listopadu 12, CZ-771 46 Olomouc, Czech Republic. E-mail: zdenek.travnicek@upol.cz*
[b]*Institute of Physical Chemistry, University of Stuttgart, Pfaffenwaldring 55, 70569 Stuttgart, Germany*

† Electronic supplementary information (ESI) available: Details of CASSCF calculations, in-phase χ_{real} and out-of-phase χ_{imag} molar susceptibilities for **1** at zero static magnetic field and in non-zero static field, and comparison between theoretical and experimental X-ray powder diffraction patterns for **1**. See DOI: 10.1039/c5dt02162f

ably, all the previously reported pentacoordinate Co(II) SMMs (**I–V**) are of the same structural type. They are composed of a tridentate *N*-donor aromatic ligand and two monodentate halido/pseudohalido ligands.

Herein, we report on the magnetic behaviour of the mononuclear compound [Co(phen)(DMSO)Cl_2] (**1**), phen = 1,10-phenanthroline, DMSO = dimethyl sulfoxide, the crystal structure of which was reported previously.[18] Interestingly, as it is apparent from the chemical formula of **1**, this compound is of a completely different structural type than compounds **I–V**, possessing a {CoN_2Cl_2O} chromophore and a combination of bidentate and monodentate ligands. The static magnetic properties were studied by temperature- and field-dependent SQUID magnetometry measurements which were analysed using the spin Hamiltonian formalism and by HF-EPR. Experimental studies were supported by theoretical calculations. Dynamic magnetic properties were studied by measuring AC susceptibility in zero and non-zero static magnetic fields.

Results and discussion

Synthesis and crystal structure

[Co(phen)(DMSO)Cl_2] compound (**1**) was prepared by recrystallization of [Co(phen)$_2$(μ-Cl)$_2$Co(Cl)$_2$] from DMSO and by slow diffusion of diethyl ether into it.[18]

It has to be stressed that all the synthetic operations must be carried out under very dry conditions for the successful preparation of **1**.[18]

The crystal structure was well described (CCDC number: 193345)[18] but some aspects will be emphasized for the purposes of this article. The geometry of a coordination polyhedron is in between a square pyramidal and a trigonal bipyramidal as can be deduced from the Addison parameter τ (τ = 0.54, τ = 0 for ideally square pyramidal and 1 for trigonal bipyramidal geometry).[19] The Co–Cl bonds (2.3100(8) and 2.3556(8) Å) are the longest metal–ligand bond lengths in the {$CoCl_2N_2O$} chromophore, while the Co–O bond is the shortest −2.052(2) Å. The Co–N bonds are dissimilar in lengths and they adopt the values of 2.119(2) and 2.169(2) Å (Fig. 1a). From the above mentioned structural parameters it is apparent that the coordination polyhedron in **1** is much distorted in view of the significant differences found in the metal–ligand bond lengths.

The crystal structure of **1** is rich in weak non-covalent intermolecular contacts such as C–H···Cl, C–H···O, or π–π stacking interactions. There are two repeating dimeric [Co(phen)-(DMSO)Cl_2]$_2$ synthons, which can be distinguished in the crystal structure of **1**. One dimer is linked by weak C–H···O hydrogen bonds (Fig. 1b, d = 3.212(4) Å, further abbreviated as syn1), while the second one is held by C–H···Cl non-covalent contacts (Fig. 1c, d = 3.710(2) Å, syn2). These two structural fragments are assembled into a ladder-like substructure by stacking the phen rings (the shortest C···C distances are 3.515(4) Å in syn1, 3.484(5) Å in syn2; in syn1 there is also a short C···N distance equal to 3.453(4) Å). The detailed discussion of intermolecular interactions in **1** is necessary, because the non-covalent contacts such as hydrogen bonds[20] or stack-

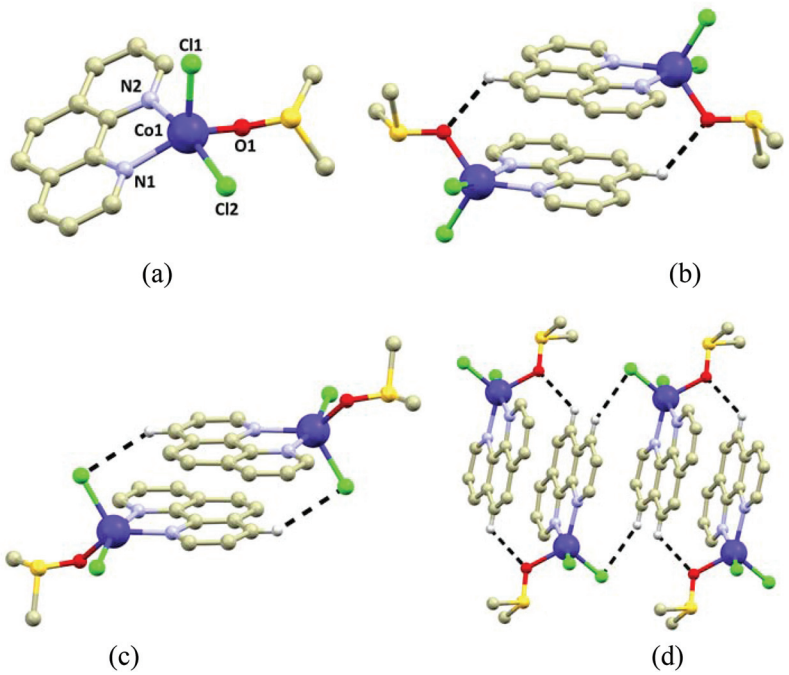

Fig. 1 Molecular structure of **1** (a). A view of a supramolecular dimer syn1 (b) and syn2 (c) *via* π–π stacking of aromatic rings and C–H···O (syn1) or C–H···Cl (syn2) non-covalent interactions (dashed lines). The overall view of a ladder-like substructure composed of [Co(phen)(DMSO)Cl_2] molecules aligned in the synthons syn1 and syn2 (d). Hydrogen atoms were omitted for clarity except for those involved in non-covalent interactions.

ing of aromatic rings[21] are capable of mediating magnetic exchange interactions which might have a strong influence on dynamic magnetic properties of SMMs.[16]

Static magnetic properties and theoretical calculations

The static magnetic properties (Fig. 2) were measured in two different ways, *i.e.* (i) as temperature dependence (1.9–300 K) of mean susceptibility and (ii) field dependence of magnetization (0–7 T). The effective magnetic moment (μ_{eff}) adopts a value close to 4.84 μ_B at room temperature which is significantly higher than the spin-only value for high-spin Co(II) with $g = 2.00$ and $S = 3/2$ ($\mu_{eff} = 3.87\ \mu_B$). This indicates a significant contribution of spin–orbit coupling to the ground state magnetic moment. Below 50 K μ_{eff} continuously decreases to approximately 3.54 μ_B, which is a sign of zero-field splitting (ZFS) of the Co^{II} atom and/or weak antiferromagnetic interactions between the individual molecules presented in the solid state.

Due to the possible mediation of antiferromagnetic interactions *via* non-covalent contacts (as mentioned above) we decided to investigate the effectivity of magnetic exchange coupling within the supramolecular dimers syn1 and syn2 (Fig. 3). This was done by broken-symmetry DFT calculations using ORCA software in order to decide which model, *i.e.* for isolated mononuclear, dimeric or polymeric compounds, would describe the magnetic properties in the best way (Fig. 1b–d). Therefore, the well-established B3LYP functional and scalar relativistic contracted version of def2-TZVP(-f) basis functions together with the zero order regular approximation (ZORA) was utilized to calculate the energy difference Δ between the high spin (HS) and broken-symmetry (BS) spin states:

$$\Delta = E_{BS} - E_{HS} \quad (1)$$

where the following spin Hamiltonian for the dimeric molecular fragments syn1 and syn2 was used:

$$\hat{H} = -J(\vec{S}_1 \cdot \vec{S}_2) \quad (2)$$

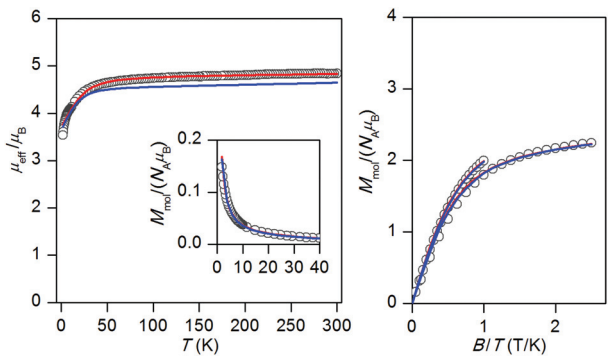

Fig. 2 Temperature dependence of the effective magnetic moment and molar magnetization measured at $B = 0.1$ T in the inset, and isothermal reduced magnetizations measured at $T = 2$ and 5 K. Empty circles: experimental data. Red full lines: calculated data using eqn (1), with $g = 2.44(1)$, $D = -17(1)$ cm^{-1}, $E/D = 0.24(5)$ cm^{-1}, $zj = -0.16(2)$ cm^{-1} and $\chi_{TIP} = 7(2) \times 10^{-9}$ m^3 mol^{-1}. Blue full lines: calculated data using the CASSCF/NEVPT2 energy levels in eqn (7).

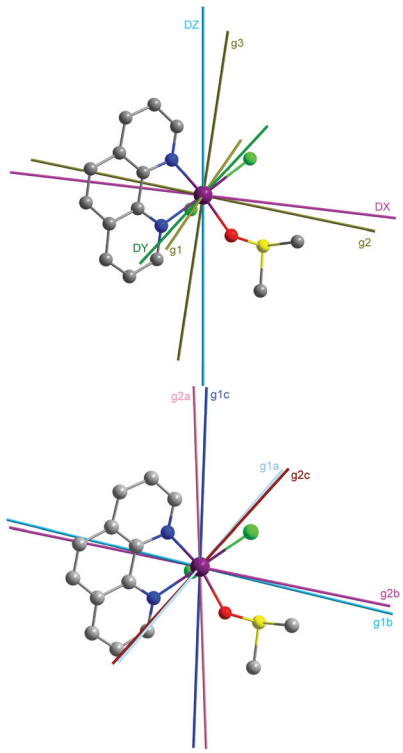

Fig. 3 Molecular structure of **1**: (a) overlaid with g-tensor and D-tensor axes derived with the spin Hamiltonian for $S = 3/2$; (b) overlaid with effective g-tensor axes derived with the spin Hamiltonian for the effective spin $S_{eff} = 1/2$ for both low-lying Kramers doublets. The hydrogen atoms were omitted for clarity.

The calculations resulted in $\Delta_{syn1} = -0.279$ cm^{-1} and $\Delta_{syn2} = +0.018$ cm^{-1}. Afterwards, the isotropic exchange J-values were calculated by Ruiz's approach[22,23] as

$$J = 2\Delta/[(S_1 + S_2)(S_1 + S_2 + 1)] \quad (3)$$

which resulted in $J_{syn1} = -0.047$ cm^{-1}, $J_{syn2} = +0.003$ cm^{-1}. It has been found out that the exchange coupling within the supramolecular dimers syn1 and syn2 is very weak and therefore the magnetic system can be considered as almost isolated.

Therefore, the following spin Hamiltonian involving the single ion axial (D) and rhombic (E) ZFS parameters, Zeeman term and molecular field correction zj was postulated[24]

$$\hat{H} = D\left(\hat{S}_z^2 - \hat{S}^2/3\right) + E\left(\hat{S}_x^2 - \hat{S}_y^2\right) + \mu_B B_a g \hat{S}_a - zj\langle\hat{S}_a\rangle\hat{S}_a \quad (4)$$

where a defines the orientation of the magnetic field vector in polar coordinates as $B_a = B(\sin\theta\cos\varphi, \sin\theta\sin\varphi, \cos\theta)$.

The molar magnetization in the a-direction of the magnetic field, M_a, was numerically calculated as:

$$M_a = -N_A \frac{\sum_i \left(\sum_k \sum_l C_{ik}^{+}(Z_a)_{kl}C_{li}\right)\exp(-\varepsilon_{a,i}/kT)}{\sum_i \exp(-\varepsilon_{a,i}/kT)} \quad (5)$$

where Z_a is the matrix element of the Zeeman term for the a-direction of the magnetic field and C are the eigenvectors

resulting from the diagonalization of the complete spin Hamiltonian matrix. The inclusion of *zj* means that the iterative procedure must be applied. The final calculated molar magnetization was calculated as an integral average in order to suitably simulate the powder sample signal.

$$M_{\mathrm{mol}} = 1/4\pi \int_0^{2\pi} \int_0^{\pi} M_a \sin\theta \,\mathrm{d}\theta \,\mathrm{d}\varphi \qquad (6)$$

Both temperature and field dependent magnetic data were fitted simultaneously in order to obtain a reliable set of parameters. As a result, negative $D = -17(1)$ cm^{-1} with a relatively large rhombicity ($E/D = 0.24(5)$) was obtained (Fig. 2).[25]

In order to support the results of the magnetic data fitting we also performed an *ab initio* calculation based on state-averaged complete-active-space self-consistent field (SA-CASSCF, the active space on metal-based d-orbitals was CAS(7,5)) wave functions complemented by N-electron valence second-order perturbation theory (NEVPT2) using ORCA software (for more detailed description of the calculations see the Experimental section).

From the list of the excited states contributing to the *D*-tensor (Tables S1 and S2, ESI†) it is apparent that the first excited state is well separated from the ground state by more than 1864 cm^{-1} and thus the spin Hamiltonian formalism is applicable.

The calculated values of the ZFS parameters were as follows: $D = -17.7$ cm^{-1} and $E/D = 0.313$ leading to the separation between the two lowest Kramers doublets equal to 40.1 cm^{-1}. These values of the single-ion ZFS parameters are in very good agreement with those determined from fitting of the experimental magnetic data ($D = -17(1)$ cm^{-1}, $E/D = 0.24(5)$ cm^{-1}). A similar quality of agreement between the theory and the experiment was also achieved for other tetracoordinate Co(II)[26] and hexacoordinate Co(II)[27] field-induced single-ion magnets, hence showing that this theoretical approach is suitable for studying Co(II) complexes in relation to their ZFS tensor and magnetic properties. Also, the *g*-tensor values were found as: $g_1 = 2.176$, $g_2 = 2.321$, $g_3 = 2.461$ resulting in $g_{\mathrm{iso}} = 2.320$. The main axes of the *g*-tensor and the *D*-tensor are depicted in Fig. 3a. It can be concluded that there is a small non-coincidence between these two tensors; despite this fact we can approximate their mutual relationship as $g_x = g_2$, $g_y = g_1$, and $g_z = g_3$. Furthermore, the two Kramers doublets were also analysed using the effective spin Hamiltonian with $S_{\mathrm{eff}} = 1/2$, and the outcome of this procedure is visualized in Fig. 3b, where g_{eff}-tensor's axis is shown. The lowest doublet has $g_{1a} = 1.546$, $g_{1b} = 2.187$, $g_{1c} = 6.774$ and the second doublet has $g_{2a} = 1.898$, $g_{2b} = 2.435$, $g_{2c} = 5.895$. Thus, both doublets have a large axial type of magnetic anisotropy, but have different orientations of easy axes.

In the next step, we utilized the respective *ab initio* CASSCF/NEVPT2 spin–orbit coupling, orbital and spin angular momentum matrices:

$$\mathbf{H} = \mathbf{H}_{\mathrm{SOC}} + \mu_{\mathrm{B}}(\mathbf{L} + g_{\mathrm{e}}\mathbf{S})\cdot\mathbf{B} \qquad (7)$$

to calculate all 120 energy levels for any orientation of the magnetic field B_a, followed by the integral calculation of both temperature and field dependent magnetization data, which are in good agreement with the experimental ones (Fig. 2).

EPR spectroscopy

We have also recorded high-frequency electron paramagnetic resonance spectra at different frequencies between 175 and 1000 GHz (Fig. 4 and S3†) with the aim of obtaining a better estimate of the *g* tensor and zero-field splitting values. At the lowest frequency of 175 GHz, three resonance lines are observed at 2.09, 4.80 and 7.27 T. With increasing frequencies, these resonance lines move to higher fields. Extrapolating the resonance line positions to zero field gives resonance frequencies close to zero. We therefore attribute the observed three resonance lines to transitions within the ground doublet along the three principal directions. Even at frequencies of 1000 GHz, we did not see any resonance line that can be attributed to interdoublet transitions. As a consequence, we cannot equivocally determine the sign and magnitude of *D*, which we have therefore fixed to the CASSCF value of $D = -17.7$ cm^{-1}. We obtained the best fit for $E/D = 0.33$, $g_x = 2.6$, $g_y = 2.4$, $g_z = 2.3$. These values differ from those obtained from the CASSCF calculation, but it must be remarked that E/D and the *g* tensor values are strongly correlated in the EPR fit.

Dynamic magnetic properties

The analysis of the static magnetic data of **1** showed that there is a uniaxial type of anisotropy, and therefore dynamic AC susceptibility data were also acquired. In the zero static magnetic field, there was no out-of-phase susceptibility signal, but the field dependent measurement performed at $T = 1.9$ K confirmed a slow relaxation of magnetization (Fig. S1, ESI†).

Therefore, AC susceptibility measurements were performed in the non-zero static field, $B_{\mathrm{dc}} = 0.1$ T at various temperatures,

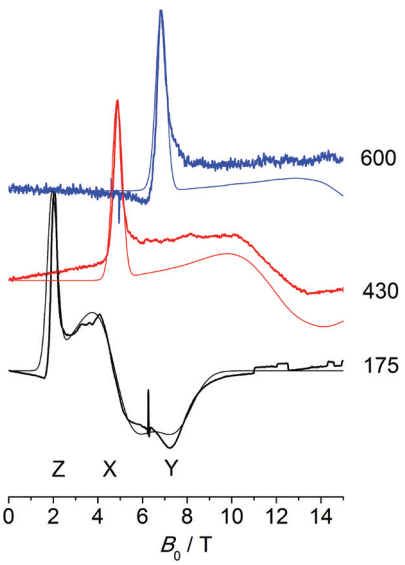

Fig. 4 HFEPR spectra recorded on pressed powder pellets of **1** at 5 K and different frequencies (in GHz) as indicated.

showing a typical pattern for slow-relaxation of magnetization typically observed for SMM species (Fig. 5). The outcome of the analysis of the AC susceptibility data for each temperature using the one-component Debye's model:

$$\chi(\omega) = \chi_S + (\chi_T - \chi_S)/[1 + (i\omega\tau)^{1-\alpha}] \quad (8)$$

are sets of isothermal (χ_T) and adiabatic (χ_S) susceptibilities, relaxation times (τ) and distribution parameters (α) (Table S4, ESI†).

Then, the Argand (Cole–Cole) plot was constructed (Fig. 5) and the Arrhenius equation was applied to analyse the temperature dependence of relaxation times, which resulted in $\tau_0 = 5.69 \times 10^{-9}$ s and the spin reversal barrier $U = 10.4$ K (7.2 cm^{-1}) (Fig. 5), where only data having maxima in the Argand diagram were used. The effective value of U is much lower than the theoretical prediction based on the parameters derived from magnetic analysis, $U_{mag} = 2(D^2 + 3E^2)^{1/2} = 52.5$ K, or from the CASSCF/NEVPT2 calculations, $U_{ab\ initio} = 57.7$ K.

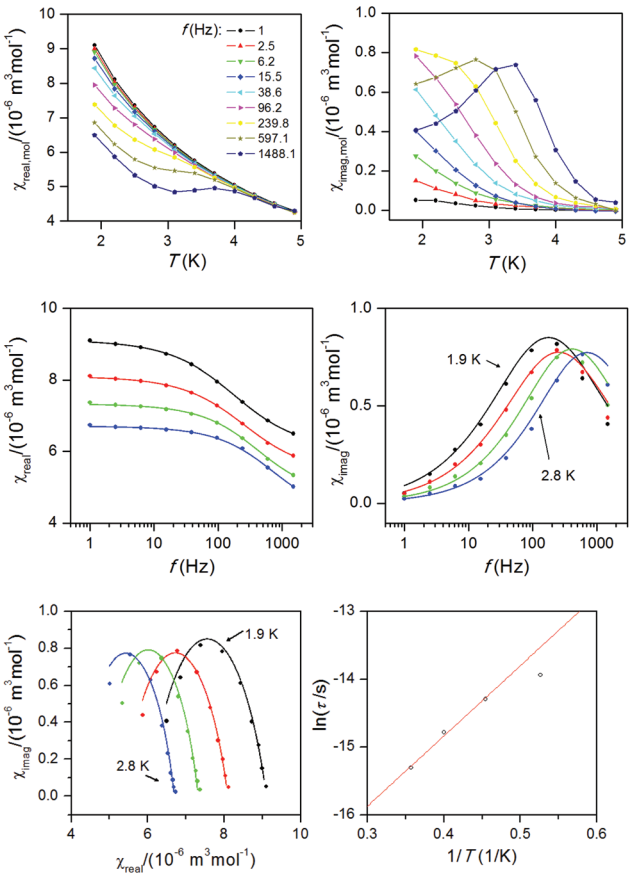

Fig. 5 Top: In-phase χ_{real} and out-of-phase χ_{imag} molar susceptibilities for **1** at the applied external field $B_{dc} = 0.1$ T. Lines serve as guides for the eyes. Middle: Frequency dependence of the in-phase χ_{real} and out-of-phase χ_{imag} molar susceptibilities for **1** at $B_{dc} = 0.1$ T. Full points – experimental data, full lines – fitted data using eqn (8). Bottom: The Argand (Cole–Cole) plot with full lines showing the fitted data using eqn (8) (left) and fit of resulting relaxation times according to the Arrhenius equation (right).

However, this kind of discrepancy is observed also in other pentacoordinate Co(II) SIMs **I–V** as listed in Table 1, and generally speaking, also for other 3d-metal SIMs reported so far.[15,28] Such lowering of spin reversal barrier is usually ascribed to the rhombic term, which causes quantum-tunnelling of magnetization and indeed we found a large rhombicity in compound **1** ($E/D = 0.24(5)$). However, we must stress here that U reflects a thermally activated Orbach mechanism, and therefore limiting the analysis of AC susceptibility data only to the data having maxima in the Argand diagram, which means that data measured between $T = 1.9$ and 2.8 K, could be also the source of reported deviation in U, because non-zero out-of-phase AC susceptibility is already observed below 5 K. Therefore, AC susceptibility data were also analysed with the simplified model[29] based on eqn (9):

$$\ln(\chi''/\chi') = \ln(2\pi f\tau_0) + U/kT \quad (9)$$

where higher temperature AC data for higher applied frequencies were included as shown in Fig. 6. As a result we obtained sets of the following parameters: $\tau_0 = 2.48 \times 10^{-10}$ s, $U = 40.3$ K for $f = 1488.1$ Hz, $\tau_0 = 1.43 \times 10^{-9}$ s, $U = 33.6$ K for $f = 597.1$ Hz, $\tau_0 = 1.06 \times 10^{-8}$ s, $U = 26.7$ K for $f = 239.8$ Hz and $\tau_0 = 5.83 \times 10^{-8}$ s, $U = 21.4$ K for $f = 96.2$ Hz. Herein, the variation of fitted parameters can be due to omitting the distribution of relaxation processes (parameter α in eqn (8)). Nevertheless, such derived U parameters are much higher (*e.g.* $U = 40.3$ K for $\nu = 1488.1$ Hz) and closer to values predicted by the spin Hamiltonian parameter.

To conclude, the relaxation processes in Co(II) SIMs are generally very complex covering apart from the Orbach process, also Raman and direct relaxation processes, influenced also by electronuclear spin entanglement, which makes the analysis of these mechanisms non-trivial.[30]

Experimental

Synthesis

All reagents and solvents were purchased from commercial sources (Sigma Aldrich) and used as received. The synthesis of $[Co(phen)_2(\mu\text{-}Cl)_2CoCl_2]$ was performed according to literature methods.[18]

Synthesis of [Co(phen)(DMSO)Cl$_2$]

0.5 g of $[Co(phen)_2(\mu\text{-}Cl)_2CoCl_2]$ was dissolved in a minimal volume of dry DMSO and then the solution was filtered through filter paper. Then the dark blue-green solution was transferred to a 15 ml flask, which was sealed by a perforated plastic cap and it was left in a 500 ml closed flask with 50 ml of diethyl ether and with a beaker full of potassium hydroxide (drying agent). After one week, the blue crystalline solid was formed, which was filtered off, washed with diethyl ether and dried in a desiccator under a stream of nitrogen. The phase purity of the sample was verified by powder X-ray diffraction analysis (ESI, Fig. S2†). Elemental analysis: $C_{14}H_{14}Cl_2Co_1N_2O_1S_1$,

Table 1 Spin Hamiltonian parameters of the studied compound **1** and other similar compounds derived from experimental magnetic data and from CASSCF/NEVPT2/ZORA/def2-TZVP(-f) calculations

Compound {chromophore}	Experimental data						*Ab initio* calculations[a,b]			
	τ	g_{iso}	D/cm^{-1}	E/D	U_{eff}/cm^{-1}	t_0/s	D/cm^{-1}	E/D	g_1, g_2, g_3, g_{iso}	$g_{eff,1}, g_{eff,2}, g_{eff,3}$
1 {CoN_2Cl_2O}	0.54	2.44(1)	−17(1)	0.24(5)	7.2	5.69×10^{-9}	−17.7	0.31	2.176, 2.321, 2.461, 2.320	1.546, 2.178, 6.774
					14.9–28.0[c]	$0.248–58.3 \times 10^{-9}$ [c]				
I {CoN_5}[10]	0.27	2.07	−28.1	—	11.1	3.6×10^{-6}	−45.1	0.18	2.078, 2.254, 2.713, 2.348	0.997, 1.284, 7.864
II {CoN_5}[10]	0.03	2.13	−28.2	—	16.7	5.1×10^{-7}	−113.5	0.13	1.836, 2.104, 3.211, 2.383	0.718, 0.875, 9.194
III {CoN_3Cl_2}[16]	0.01	2.85	+151	0.08	6.4	3.1×10^{-9}	−120.2	0.11	1.718, 1.927, 3.304, 2.316	0.687, 0.771, 9.328
IV {CoN_3Cl_2}[16]	0.05	—	—	—	19.5	1.1×10^{-6}	−106.6	0.13	1.819, 2.072, 3.234, 2.375	0.859, 0.994, 9.163
V {CoN_5}[17]	0.43	—	—	—	11.8	5.9×10^{-6}	+40.3	0.23	1.990, 2.274, 2.478, 2.247	1.718, 2.952, 6.345

[a] D, E and g_1, g_2, g_3, g_{iso} correspond to the spin Hamiltonian with $S = 3/2$ (eqn (4)). It has to be noted that the first excited states are relatively close to the ground state – see Table S1 (ESI). [b] $g_{eff,1}$, $g_{eff,2}$, $g_{eff,3}$ correspond to the Kramers doublet ground state with effective spin $S_{eff} = 1/2$. [c] The parameters calculated using eqn (9).

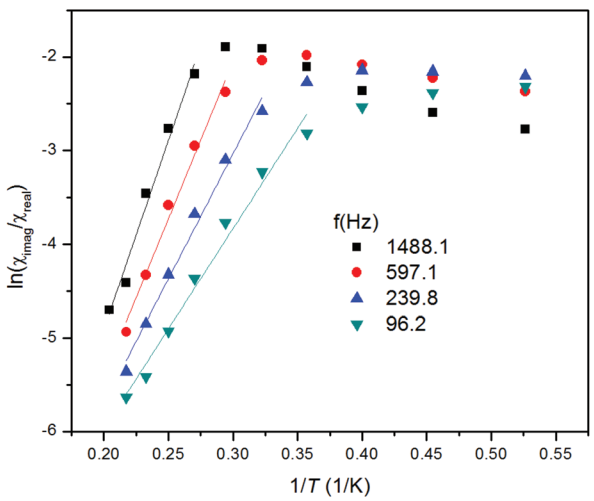

Fig. 6 Analysis of in-phase χ_{real} and out-of-phase χ_{imag} molar susceptibilities for **1** measured at the applied external field B_{dc} = 0.1 T according to eqn (9). Full points – experimental data, full lines – calculated data.

M_r = 388.2, found: C, 43.4; H, 3.6; N, 7.0; requires: C, 43.3; H, 3.6; N, 7.2.

Physical methods

Elemental analysis (C, H, N) was performed on a Flash 2000 CHNO-S Analyzer (Thermo Scientific). Temperature dependence of the magnetization at B = 0.1 T from 1.9 to 300 K and the isothermal magnetizations at T = 2.0 and 5.0 K up to B = 5 T were measured using a MPMS XL-7 SQUID magnetometer (Quantum Design). The experimental data were corrected for diamagnetism. Measurements of AC susceptibility were carried out in a 3.8 Oe ac field oscillating at various frequencies from 1 to 1500 Hz and with various dc fields. The X-ray powder diffraction patterns of all solid samples were recorded on a Mini-Flex600 (Rigaku) instrument equipped with the Bragg–Brentano geometry, and with iron-filtered Cu Kα 1,2 radiation.

High-frequency EPR spectra were recorded on a home-built spectrometer. Its radiation source is a 0–20 GHz signal generator (Anritsu or VDI) in combination with an amplifier–multiplier chain (VDI) to obtain the required frequencies (80–1100 GHz). It features a quasi-optical bridge (Thomas Keating) and induction mode detection. The detector is a QMC Instruments magnetically tuned InSb hot electron bolometer. The sample is located in an Oxford Instruments 15/17 T cryomagnet equipped with a variable temperature insert (1.5–300 K). The spectrometer control programme was written in LabView.

Theoretical methods

All theoretical calculations were performed with the ORCA 3.0 computational package.[31] All the calculations employed the scalar relativistic contracted version of def2-TZVP(-f) basis functions[32] together with the zero order regular approximation (ZORA)[33] and also utilized the chain-of-sphere (RIJCOSX) approximation to exact exchange.[34] DFT calculations were based on the B3LYP functional.[35] The ZFS and g tensors were calculated by using self-consistent field (SA-CASSCF) wave functions[36] complemented by N-electron valence second order perturbation theory (NEVPT2).[37] The active space of the CASSCF calculation was set to five d-orbitals of Co(II) (CAS (7,5)). The ZFS parameters, based on dominant spin–orbit coupling contributions from excited states, were calculated through quasi-degenerate perturbation theory (QDPT),[38] in which approximations to the Breit–Pauli form of the spin–orbit coupling operator (SOMF approximation)[39] and the effective Hamiltonian theory[40] were utilized.

Conclusions

In this article, we reported results of thorough structural and magnetic analyses of [Co(phen)(DMSO)Cl_2] (**1**). It has been revealed that this compound has large and negative magnetic anisotropy (D = −17(1) cm^{-1}) and a very large rhombicity (E/D = 0.24(5)) as derived from spin Hamiltonian analysis of temperature and field dependent magnetic data. These results were supported by the HF-EPR measurements; however, in the frequency range of 150–1000 GHz any resonance arising from an interdoublet transition was not observed. Thus we were not able to determine sign and magnitude of the zero-field splitting parameters, but a very large rhombicity was confirmed (E/D_{EPR} = 0.33). *Ab initio* calculations are in agreement with the experimentally derived zero-field splitting parameters: D_{calc} = −17.1 cm^{-1}, E/D_{calc} = 0.31.

Dynamic magnetic properties revealed that **1** behaves as a field-induced single molecule magnet with either energy of spin reversal barrier (U_{eff} = 10.4 K) and fast relaxation time (τ_0 = 5.69 × 10^{-9} s) according to analysis of the Argand diagram and the one-component Debye model (eqn (8)), or with U_{eff} = 21.4–40.3 K and τ_0 = 0.248–58.3 × 10^{-9} s according to the simplified model (eqn (9)). To conclude, compound **1** represents a first example of a pentacoordinate Co(II) single-ion magnet with the {$CoCl_2N_2O$} chromophore and it must be stressed that this compound differs structurally from all the previously reported pentacoordinate Co(II) single-molecule magnets.[10,16,17] Thus, this report deals with the magnetic properties of a new type of pentacoordinate Co(II) single-molecule magnet.

Acknowledgements

We acknowledge financial support from the Grant Agency of the Czech Republic (GAČR 13-27355P), the National Programme of Sustainability I (LO1305) of the Ministry of Education, Youth and Sports of the Czech Republic, and the Czech-German FP6-Mobility-9 project 7AMB15DE002 and DFG SPP1601.

Notes and references

1 R. Boča, *Coord. Chem. Rev.*, 2004, **248**, 757–815.
2 (*a*) A. Caneschi, D. Gatteschi, R. Sessoli, A. L. Barra, L. C. Brunel and M. Guillot, *J. Am. Chem. Soc.*, 1991, **113**, 5873–5874; (*b*) R. Sessoli, D. Gatteschi, A. Caneschi and M. A. Novak, *Nature*, 1993, **365**, 141–143.
3 N. Ishikawa, M. Sugita, T. Ishikawa, S.-y. Koshihara and Y. Kaizu, *J. Am. Chem. Soc.*, 2003, **125**, 8694–8695.
4 (*a*) O. Waldmann, *Inorg. Chem.*, 2007, **46**, 10035–10037; (*b*) F. Neese and D. A. Pantazis, *Faraday Discuss.*, 2011, **148**, 229–238.
5 (*a*) J. M. Zadrozny, D. J. Xiao, J. R. Long, M. Atanasov, F. Neese, F. Grandjean and G. J. Long, *Inorg. Chem.*, 2013, **52**, 13123–13131; (*b*) J. M. Zadrozny, D. J. Xiao, M. Atanasov, G. J. Long, F. Grandjean, F. Neese and J. R. Long, *Nat. Chem.*, 2013, **5**, 577–581.
6 (*a*) J. M. Zadrozny, M. Atanasov, A. M. Bryan, C.-Y. Lin, B. D. Rekken, P. P. Power, F. Neese and J. R. Long, *Chem. Sci.*, 2013, **4**, 125–138; (*b*) C. Mathonière, H.-J. Lin, D. Siretanu, R. Clérac and J. M. Smith, *J. Am. Chem. Soc.*, 2013, **135**, 19083–19086; (*c*) X. Feng, C. Mathonière, I.-R. Jeon, M. Rouzières, A. Ozarowski, M. L. Aubrey, M. I. Gonzalez, R. Clérac and J. R. Long, *J. Am. Chem. Soc.*, 2013, **135**, 15880–15884; (*d*) W. H. Harman, T. D. Harris, D. E. Freedman, H. Fong, A. Chang, J. D. Rinehart, A. Ozarowski, M. T. Sougrati, F. Grandjean, G. J. Long, J. R. Long and C. J. Chang, *J. Am. Chem. Soc.*, 2010, **132**, 18115–18126; (*e*) D. E. Freedman, W. H. Harman, T. D. Harris, G. J. Long, C. J. Chang and J. R. Long, *J. Am. Chem. Soc.*, 2010, **132**, 1224–1225; (*f*) D. Weismann, Y. Sun, Y. Lan, G. Wolmershäuser, A. K. Powell and H. Sitzmann, *Chem. – Eur. J.*, 2011, **17**, 4700–4704.
7 S. Mossin, B. L. Tran, D. Adhikari, M. Pink, F. W. Heinemann, J. Sutter, R. K. Szilagyi, K. Meyer and D. J. Mindiola, *J. Am. Chem. Soc.*, 2012, **134**, 13651–13661.
8 R. C. Poulten, M. J. Page, A. G. Algarra, J. J. Le Roy, I. López, E. Carter, A. Llobet, S. A. Macgregor, M. F. Mahon, D. M. Murphy, M. Murugesu and M. K. Whittlesey, *J. Am. Chem. Soc.*, 2013, **135**, 13640–13643.
9 (*a*) R. Ishikawa, R. Miyamoto, H. Nojiri, B. K. Breedlove and M. Yamashita, *Inorg. Chem.*, 2013, **52**, 8300–8302; (*b*) G. A. Craig, J. J. Marbey, S. Hill, O. Roubeau, S. Parsons and M. Murrie, *Inorg. Chem.*, 2014, **54**, 13–15; (*c*) J. Vallejo, A. Pascual-Álvarez, J. Cano, I. Castro, M. Julve, F. Lloret, J. Krzystek, G. De Munno, D. Armentano, W. Wernsdorfer, R. Ruiz-García and E. Pardo, *Angew. Chem., Int. Ed.*, 2013, **52**, 14075–14079.
10 T. Jurca, A. Farghal, P.-H. Lin, I. Korobkov, M. Murugesu and D. S. Richeson, *J. Am. Chem. Soc.*, 2011, **133**, 15814–15817.
11 See *e.g.*: (*a*) R. Boča, J. Miklovič and J. Titiš, *Inorg. Chem.*, 2014, **53**, 2367–2369; (*b*) D.-K. Cao, J.-Q. Feng, M. Ren, Y.-W. Gu, Y. Song and M. D. Ward, *Chem. Commun.*, 2013, **49**, 8863–8865; (*c*) J. M. Zadrozny, J. Liu, N. A. Piro, C. J. Chang, S. Hill and J. R. Long, *Chem. Commun.*, 2012, **48**, 3927–3929; (*d*) J. M. Zadrozny and J. R. Long, *J. Am. Chem. Soc.*, 2011, **133**, 20732–20734; (*e*) M. Idešicová and R. Boča, *Inorg. Chim. Acta*, 2013, **408**, 162–171; (*f*) M. Idešicová, Ľ. Dlháň, J. Moncoľ, J. Titiš and R. Boča, *Polyhedron*, 2012, **36**, 79–84; (*g*) M. Idešicová, J. Titiš, J. Krzystek and R. Boča, *Inorg. Chem.*, 2013, **52**, 9409–9417.
12 See *e.g.*: (*a*) N. Nedelko, A. Kornowicz, I. Justyniak, P. Aleshkevych, D. Prochowicz, P. Krupiński, O. Dorosh, A. Ślawska-Waniewska and J. Lewiński, *Inorg. Chem.*, 2014, **53**, 12870–12876; (*b*) R. Ruamps, L. J. Batchelor, R. Guillot, G. Zakhia, A.-L. Barra, W. Wernsdorfer, N. Guihery and T. Mallah, *Chem. Sci.*, 2014, **5**, 3418–3424; (*c*) D. M. Pinero Cruz, D. N. Woodruff, I.-R. Jeon, I. Bhowmick, M. Secu, E. A. Hillard, P. Dechambenoit and R. Clerac, *New J. Chem.*,

2014, **38**, 3443–3448; (*d*) C. Rajnák, J. Titiš, I. Šalitroš, R. Boča, O. Fuhr and M. Ruben, *Polyhedron*, 2013, **65**, 122–128.

13 (*a*) V. Chandrasekhar, A. Dey, A. J. Mota and E. Colacio, *Inorg. Chem.*, 2013, **52**, 4554–4561; (*b*) Y.-Y. Zhu, C. Cui, Y.-Q. Zhang, J.-H. Jia, X. Guo, C. Gao, K. Qian, S.-D. Jiang, B.-W. Wang, Z.-M. Wang and S. Gao, *Chem. Sci.*, 2013, **4**, 1802–1806; (*c*) J. Vallejo, I. Castro, R. Ruiz-García, J. Cano, M. Julve, F. Lloret, G. De Munno, W. Wernsdorfer and E. Pardo, *J. Am. Chem. Soc.*, 2012, **134**, 15704–15707; (*d*) J. Vallejo, I. Castro, R. Ruiz-García, J. Cano, M. Julve, F. Lloret, G. De Munno, W. Wernsdorfer and E. Pardo, *J. Am. Chem. Soc.*, 2012, **134**, 15704–15707.

14 (*a*) X.-C. Huang, C. Zhou, D. Shao and X.-Y. Wang, *Inorg. Chem.*, 2014, **53**, 12671–12673.

15 G. A. Craig and M. Murrie, *Chem. Soc. Rev.*, 2015, **44**, 2135–2147.

16 C. Rajnák, J. Titiš, O. Fuhr, M. Ruben and R. Boča, *Inorg. Chem.*, 2014, **53**, 8200–8202.

17 F. Habib, O. R. Luca, M. K. Takase, R. H. Crabtree and M. Murugesu, *Angew. Chem., Int. Ed.*, 2013, **52**, 11290.

18 B. Brewer, N. Brooks, S. Abdul-Halim and A. Sykes, *J. Chem. Crystallogr.*, 2003, **33**, 651–662.

19 A. W. Addison, T. N. Rao, J. Reedijk, J. Vanrijn and G. C. Verschoor, *J. Chem. Soc., Dalton Trans.*, 1984, 1349–1356.

20 (*a*) E. Pardo, M. Verdaguer, P. Herson, H. Rousseliere, J. Cano, M. Julve, F. Lloret and R. Lescouezec, *Inorg. Chem.*, 2011, **50**, 6250; (*b*) I. Nemec, R. Herchel, I. Šalitroš, Z. Trávníček, J. Moncoľ, H. Fuess, M. Ruben and W. Linert, *CrystEngComm*, 2012, **14**, 7015; (*c*) I. Nemec, R. Herchel, T. Silha and Z. Trávníček, *Dalton Trans.*, 2014, **43**, 15602–15616; (*d*) D. Valigura, J. Moncol, M. Korabik, Z. Pučekova, T. Lis, J. Mrozinski and M. Melnik, *Eur. J. Inorg. Chem.*, 2006, 3813; (*e*) Z. Vasková, J. Moncoľ, M. Korábik, D. Valigura, J. Švorec, T. Lis, M. Valko and M. Melník, *Polyhedron*, 2010, **29**, 154–163; (*f*) J. S. Costa, N. A. G. Bandeira, B. Le Guennic, V. Robert, P. Gamez, G. Chastanet, L. Ortiz-Frade and L. Gasque, *Inorg. Chem.*, 2011, **50**, 5696–5705.

21 Y.-H. Chi, J.-M. Shi, H.-N. Li, W. Wei, E. Cottrill, N. Pan, H. Chen, Y. Liang, L. Yu, Y.-Q. Zhang and C. Hou, *Dalton Trans.*, 2013, **42**, 15559–15569.

22 E. Ruiz, J. Cano, S. Alvarez and P. Alemany, *J. Comput. Chem.*, 1999, **20**, 1391–1400.

23 E. Ruiz, A. Rodriguez-Fortea, J. Cano, S. Alvarez and P. Alemany, *J. Comput. Chem.*, 2003, **24**, 982–989.

24 R. Boča, *A Handbook of Magnetochemical Formulae*, Elsevier, Amsterdam, 2012.

25 The standard deviations were calculated as $\sigma_i = (P_{ii}^{-1} \cdot S/(N - k))^{-1/2}$, where $P_{ij} = \Sigma(\delta\mu_n/\delta a_i \cdot \delta\mu_n/\delta a_j)$ and $S = \sum(\mu_n - \mu_n^{\exp})^2$ with $n = 1$ to N; a_i and a_j are fitted parameters, N is the number of experimental points (a sum of temperature and field dependent data), μ_n and $\mu_n^{\exp}$ are the calculated and experimental effective magnetic moments for a given temperature and magnetic field. The σ_i was then multiplied by Student's $t_{95\%}$ to provide confidence limits with 95% probabilities listed in the text.

26 I. Nemec, R. Herchel and Z. Trávníček, *Sci. Rep.*, 2015, **5**, 10761.

27 R. Herchel, L. Váhovská, I. Potočňák and Z. Trávníček, *Inorg. Chem.*, 2014, **53**, 5896–5898.

28 S. Gómez-Coca, D. Aravena, R. Morales and E. Ruiz, *Coord. Chem. Rev.*, 2015, **289–290**, 379–392.

29 (*a*) J. Bartolomé, G. FIloti, V. Kuncser, G. Schinteie, V. Mereacre, C. E. Anson, A. K. Powell, D. Prodius and C. Turta, *Phys. Rev. B: Condens. Matter*, 2009, **80**, 014430; (*b*) R. Ishikawa, R. Miyamoto, H. Nojiri, B. K. Breedlove and M. Yamashita, *Inorg. Chem.*, 2013, **52**, 8300–8302.

30 S. Gómez-Coca, A. Urtizberea, E. Cremades, P. J. Alonso, A. Camón, E. Ruiz and F. Luis, *Nat. Commun.*, 2015, **5**, 4300.

31 F. Neese, *WIREs Comput. Mol. Sci.*, 2012, **2**, 73–78.

32 D. A. Pantazis, X.-Y. Chen, C. R. Landis and F. Neese, *J. Chem. Theor. Comput.*, 2008, **4**, 908–919.

33 (*a*) E. Vanlenthe, E. J. Baerends and J. G. Snijders, *J. Chem. Phys.*, 1993, **99**, 4597–4610; (*b*) C. van Wullen, *J. Chem. Phys.*, 1998, **109**, 392–399.

34 F. Neese, F. Wennmohs, A. Hansen and U. Becker, *Chem. Phys.*, 2009, **356**, 98–109.

35 (*a*) C. Lee, W. Yang and R. G. Parr, *Phys. Rev. B: Condens. Matter*, 1988, **37**, 785; (*b*) A. D. Becke, *J. Chem. Phys.*, 1993, **98**, 1372; (*c*) A. D. Becke, *J. Chem. Phys.*, 1993, **98**, 5648; (*d*) P. J. Stephens, F. J. Devlin, C. F. Chabalowski and M. J. Frisch, *J. Phys. Chem.*, 1994, **98**, 11623.

36 P. A. Malmqvist and B. O. Roos, *Chem. Phys. Lett.*, 1989, **155**, 189–194.

37 (*a*) C. Angeli, R. Cimiraglia, S. Evangelisti, T. Leininger and J. P. Malrieu, *J. Chem. Phys.*, 2001, **114**, 10252–10264; (*b*) C. Angeli, R. Cimiraglia and J. P. Malrieu, *Chem. Phys. Lett.*, 2001, **350**, 297–305; (*c*) C. Angeli, R. Cimiraglia and J. P. Malrieu, *J. Chem. Phys.*, 2002, **117**, 9138–9153; (*d*) C. Angeli, S. Borini, M. Cestari and R. Cimiraglia, *J. Chem. Phys.*, 2004, **121**, 4043–4049; (*e*) C. Angeli, B. Bories, A. Cavallini and R. Cimiraglia, *J. Chem. Phys.*, 2006, **124**, 054108.

38 D. Ganyushin and F. Neese, *J. Chem. Phys.*, 2006, **125**, 024103.

39 F. Neese, *J. Chem. Phys.*, 2005, **122**, 034107.

40 R. Maurice, R. Bastardis, C. de Graaf, N. Suaud, T. Mallah and N. Guihéry, *J. Chem. Theor. Comput.*, 2009, **5**, 2977–2984.